

Second harmonic generation from precise diamond blade diced ridge waveguides

Hui Xu(徐慧), Ziqi Li(李子琦), Chi Pang(逄驰), Rang Li(李让), Genglin Li(李庚霖), Sh. Akhmadaliev, Shengqiang Zhou(周生强), Qingming Lu(路庆明), Yuechen Jia(贾曰辰), and Feng Chen(陈峰)

Citation: Chin. Phys. B, 2022, 31 (**9**): 094209. DOI: 10.1088/1674-1056/ac5242
Journal homepage: http://cpb.iphy.ac.cn; http://iopscience.iop.org/cpb

What follows is a list of articles you may be interested in

Broadband and efficient second harmonic generation in $LiNbO_3$-$LiTaO_3$ composite ridge waveguides at telecom-band

Xin-Tong Zhang(张欣桐)
Chin. Phys. B, 2021, 30 (**1**): 014205. DOI: 10.1088/1674-1056/abb232

Design of an augmented reality display based on polarization grating

Renjie Xia(夏人杰), Changshun Wang(王长顺), Yujia Pan(潘雨佳), Tianyu Chen(陈天宇), Ziyao Lyu(吕子瑶), Lili Sun(孙丽丽)
Chin. Phys. B, 2019, 28 (**7**): 074201. DOI: 10.1088/1674-1056/28/7/074201

Enhanced second harmonic generation in a two-dimensional optical micro-cavity

Jian-Jun Zhang(张建军), Hui-Fang Wang(王慧芳), Jun-Hua Hou(候俊华)
Chin. Phys. B, 2018, 27 (**3**): 034207. DOI: 10.1088/1674-1056/27/3/034207

Tunable second harmonic generation from a Kerr-lens mode-locked Yb: $YCa_4O(BO_3)_3$ femtosecond laser

Zi-Ye Gao(高子叶), Jiang-Feng Zhu(朱江峰), Zheng-Mao Wu(吴正茂), Zhi-Yi Wei(魏志义), Hao-Hai Yu(于浩海), Huai-Jin Zhang(张怀金), Ji-Yang Wang(王继扬)
Chin. Phys. B, 2017, 26 (**4**): 044202. DOI: 10.1088/1674-1056/26/4/044202

Correction of walk-off-induced wavefront distortion for continuous-wave laser

Hongxin Zou(邹宏新), Guozhu Chen(陈国柱), Yue Wu(伍越), Yong Shen(沈咏), Qu Liu(刘曲)
Chin. Phys. B, 2016, 25 (**9**): 094211. DOI: 10.1088/1674-1056/25/9/094211

Second harmonic generation from precise diamond blade diced ridge waveguides

Hui Xu(徐慧)[1], Ziqi Li(李子琦)[1,2], Chi Pang(逄驰)[1], Rang Li(李让)[1,3], Genglin Li(李庚霖)[1], Sh. Akhmadaliev[3], Shengqiang Zhou(周生强)[3], Qingming Lu(路庆明)[4], Yuechen Jia(贾曰辰)[1,†], and Feng Chen(陈峰)[1]

[1] *School of Physics, State Key Laboratory of Crystal Materials, Shandong University, Jinan* 250100, *China*
[2] *Division of Physics and Applied Physics, School of Physical and Mathematical Sciences, Nanyang Technological University, Singapore* 637371, *Singapore*
[3] *Institute of Ion Beam and Materials Research, Helmholtz-Zentrum Dresden-Rossendorf, Dresden* 01314, *Germany*
[4] *School of Chemistry and Chemical Engineering, Shandong University, Jinan* 250100, *China*

(Received 8 November 2021; revised manuscript received 18 January 2022; accepted manuscript online 7 February 2022)

Carbon ion irradiation and precise diamond blade dicing are applied to fabricate Nd:GdCOB ridge waveguides. The propagation properties of the fabricated Nd:GdCOB waveguides are investigated through experiments and theoretical analysis. Micro-Raman analysis reveals that the Nd:GdCOB crystal lattice expands during the irradiation process. Micro-second harmonic spectroscopic analysis suggests that the original nonlinear properties of the Nd:GdCOB crystal are greatly enhanced within the waveguide volume. Under pulsed 1064 nm laser pumping, second harmonic generation (SHG) at 532 nm has been achieved in the fabricated waveguides. The maximum SHG conversion efficiencies are determined to be $\sim 8.32\ \%\cdot W^{-1}$ and $\sim 22.36\ \%\cdot W^{-1}$ for planar and ridge waveguides, respectively.

Keywords: optical waveguides, Nd:GdCOB crystal, second harmonic generation

PACS: 42.79.Gn, 42.70.Mp, 42.65.–k **DOI:** 10.1088/1674-1056/ac5242

1. Introduction

Optical waveguides, as one of the essential components of integrated photonics, can confine light fields in extremely small volumes.[1,2] As a result, the light intensity obtained from the waveguide volume is much higher than that in the bulk.[3–5] This feature provides meaningful advantages in nonlinear optical applications, where various nonlinear phenomena can be generated from the waveguide structure at a relatively low optical power. For example, frequency conversion processes based on waveguides feature higher conversion efficiencies and more flexible mode selection compared with those based on bulks.[4] Combining the versatility of multifunctional crystals with the compact geometries of waveguide structures, crystalline waveguides can be used to construct multifunctional optical devices with small footprints, such as on-chip lasers, compact optical modulators and nonlinear wavelength converters.[6,7] In practice, channel or ridge waveguides with light field confinement in two dimensions (2D) are preferred to one-dimensional (1D) planar waveguides due to their better optical confinement and more flexible geometry.[8]

Ion implantation, as an important method for material modification, has been applied to a variety of crystals.[9–15] By bombarding the target crystal surface with energetic ion beams, localized lattice damage and refractive index modification appear at near-surface regions, resulting in the formation of an optical waveguide.[16–18] Up to now, this technique has been applied to the preparation of waveguides in dozens of crystalline materials.[8,16] Optical waveguides manufactured by ion implantation are generally 1D planar structures. Additional surface microfabrication is therefore needed to obtain 2D waveguide structures. Of the techniques used for surface microfabrication, femtosecond laser direct writing (FsLDW) and precise diamond blade dicing are the most common. Both techniques have been utilized to manufacture ridge waveguides based on ion-irradiated Nd:YAG planar waveguides.[19–23] However, compared with the ridge waveguides fabricated by FsLDW, those prepared by precise diamond blade dicing feature lower scattering losses and a higher optical quality owing to their smoother side walls.[19,24–26]

Combining the lasing and luminescence characteristics of Nd^{3+} ions with the nonlinear optical properties of a $GdCa_4O(BO_3)_3$ (GdCOB) matrix, it is shown that neodymium-doped GdCOB (Nd:GdCOB) has attractive optical properties as an excellent laser gain medium and an efficient self-frequency doubling (SFD) crystal.[27–31] In previous works, planar and channel waveguides have been fabricated in Nd:GdCOB crystals by ion irradiation[32] and FsLDW,[33] and second harmonic generation (SHG) has also been achieved using these waveguide structures. However, up to now, Nd:GdCOB ridge waveguides produced by ion irradiation and precise diamond dicing have not been reported.

In this work, we demonstrate the fabrication of Nd:GdCOB ridge waveguides by combining ion beam irradiation with precise diamond blade dicing techniques. We performed SHG at 532 nm in both ridge and planar waveguides

†Corresponding author. E-mail: yuechen.jia@sdu.edu.cn

© 2022 Chinese Physical Society and IOP Publishing Ltd

using 1064 nm pulsed fundamental waves.

2. Experiments

The 8 at.% Nd-doped GdCOB crystal used in this work was cut to satisfy type-I phase matching conditions ($\theta = 161.5°$, $\phi = 0°$) with dimensions of 11 mm × 9 mm × 2.2 mm. The crystal facets of 11 mm × 9 mm and 11 mm × 2.2 mm were well polished to an optical grade. As Fig. 1(a) shows, the surface of the sample was irradiated by carbon (C^{5+}) ions with an energy of 15 MeV at a fluence of 2×10^{14} ions·cm^{-2}. As a result, a planar waveguide with a thickness of ∼ 10 μm (according to the microscopic image and the ion irradiation calculations, as presented in the next section) was achieved. Ion irradiation was accomplished using the 3 MV tandem accelerator at Helmholtz-Zentrum Dresden-Rossendorf, Germany. To reduce the channel effect, the incident ion beam was deviated by 7° from the normal to the sample surface. After that, based on the planar configuration, we constructed ridge waveguides using diamond blade dicing (see Fig. 1(b)). During this process, several air grooves perpendicular to the crystal surface with a size of approximately 11 mm × 2.2 mm were produced with the blade (DISCO Corp., P1A851 SD3000R10B10)[34] installed on a precision dicing machine (Jingchuang Advanced, AR3000). The rotation and movement velocities were set to 20000 rpm and 0.05 mm·s^{-1}, respectively. With vertical optical confinement provided by the ion-induced change in refractive index and lateral optical confinement offered by two neighboring grooves, ridge waveguides with widths of 10 μm (WG1), 20 μm (WG2), 25 μm (WG3), and 30 μm (WG4) were formed. Both irradiation and precise diamond blade dicing are high-precision and repeatable waveguide construction techniques,[35–37] so that the waveguides are constructed with good stability.

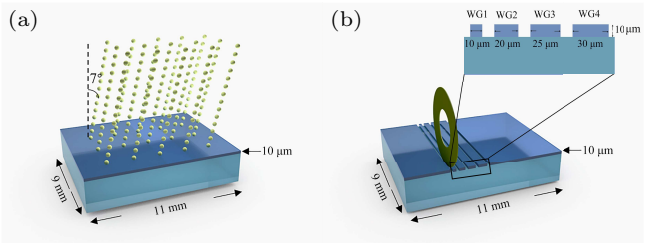


Fig. 1. Schematic illustrations of (a) 15 MeV C^{5+} ion irradiation and (b) precise diamond blade dicing for Nd:GdCOB ridge waveguide fabrication.

After fabrication, micro-Raman measurements were carried out using a spectrometer (Horiba/Jobin Yvon HR800) to investigate the microstructural modification of Nd:GdCOB crystal. With a detected range of 50 cm^{-1}–1500 cm^{-1}, a laser beam at 473 nm was focused on the waveguide cross sections and bulk at room temperature.

Micro-second harmonic (μ-SH) spectroscopic analysis of the sample was performed to evaluate the nonlinear properties of the waveguides using a confocal microscopy testing platform. A laser beam (with a pulse duration of ∼ 20 ns, a pulse energy of ∼ 2 μJ and a pulse repetition rate of ∼ 5 MHz) at 1030 nm produced by a microjoule ultrafast fiber laser system (ANTAUS-10W-2u/5M) was coupled to the sample with a 100× objective [numerical aperture (NA) = 0.3]. The reflected μ-SH signal was collected by the same objective, and after passing through several mirrors and lenses the signal was detected by a spectrometer.

As shown in Fig. 2(a), we performed SHG characterization experiments based on an end-face coupling arrangement. After the 1064 nm light beam was emitted from the pulsed laser (with a pulse width of ∼ 11.05 ns, a pulse energy of ∼ 80 μJ and a repetition rate of ∼ 5 kHz), its power and polarization were adjusted by a neutral density filter and a half-wave plate, respectively. A microscope objective (25×, NA = 0.4) was used for optical in-coupling. The SHG and residual fundamental signal outputs from the waveguides were collected by another microscope objective. In order to detect the SHG signal, we used a spectrometer and a powermeter behind an optical low-pass filter, which has a transmittance of ∼ 98% at 532 nm and a reflectivity of > 99% at 1064 nm. Figures 2(b)–2(e) present the fundamental modes along transverse magnetic (TM) and second harmonic (SH) modes along transverse electric (TE) directions in planar and WG3 ridge waveguides (all the ridge waveguides show similar modal distributions). Both fundamental and SH waves are well confined in the waveguiding regions, showing nearly single-mode profiles, which are very beneficial for SHG.

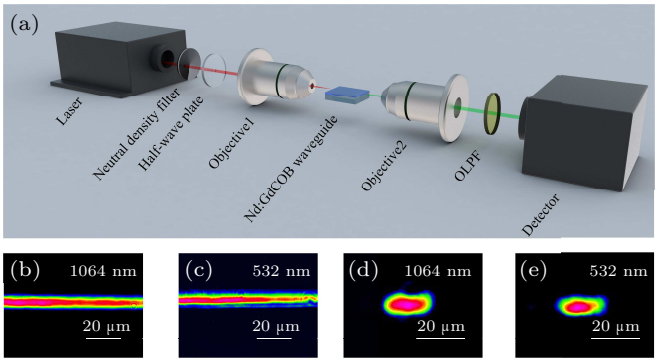


Fig. 2. (a) The end-face coupling arrangement for SHG characterization of Nd:GdCOB waveguides. The mode field distribution of planar and WG3 ridge waveguides at 1064 nm [(b), (d)] and at 532 nm [(c), (e)] (OLPF, optical low-pass filter).

3. Results and discussion

The nuclear (S_n) and electronic (S_e) stopping power profiles of 15 MeV C^{5+} ions in Nd:GdOCB were calculated using the SRIM-2008 (Stopping and Range of Ions in Matter 2008) code, and the results are shown in Fig. 3(a). A non-zero S_e is observed within the ion penetration range of 0 μm–10 μm, peaking at approximately 1.7 keV·nm^{-1} with a depth value

of ~ 6.7 μm. In contrast, the S_n value remains zero within the first 9 μm below the surface and reaches a maximum of 0.16 keV·nm^{-1} around 10 μm beneath the surface. Therefore, the electronic damage is considered to be the main cause for the change in refractive index in the ion-irradiated area, whereas the nuclear damage at the end of the ion trajectory is responsible for the creation of the optical barrier. Moreover, the formation of the waveguide layer is a collective effect of both S_n and S_e. The maximum modification of refractive index in the waveguide region is about 0.003 estimated by the formula

$$\Delta n = \frac{\sin^2 \Theta_m}{2n}, \tag{1}$$

where Θ_m is the maximum incident angle at which the laser beam cannot be focused into the waveguide by the microscope objective and $n = 1.7184$ is the refractive index of the Nd:GdCOB crystal.[32] Therefore, taking the stopping power profiles as references, we reconstructed the refractive index distribution (see Fig. 3(a)). Figures 3(b) and 3(e) demonstrate the microscopic images of the planar waveguide and the WG2 ridge waveguide, respectively. The thickness of the modified layer is observed to be around 10 μm, which is in fairly good agreement with the calculation performed using the SRIM-2008 code.[38] We imported the index profile into Rsoft Beam PROP 8.0[39] and simulated the near-field modal distribution. Taking a planar waveguide and WG2 ridge waveguide as examples, figures 3(c) and 3(f) display the simulated near-field distributions at 1064 nm, which are very similar to the experimental results imaged by a CCD camera in the end-face coupling setup (see Figs. 3(d) and 3(g)), suggesting the reasonability of the reconstructed refractive index profile.

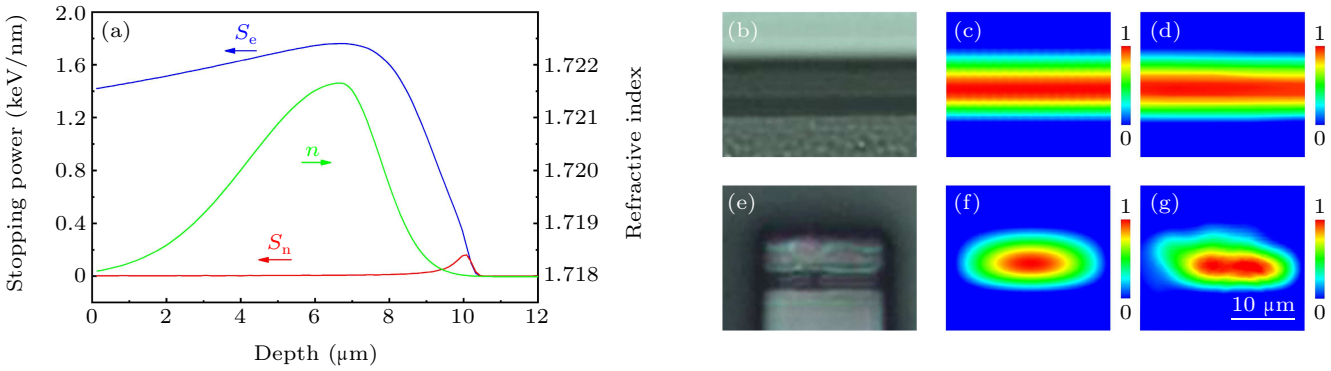


Fig. 3. (a) The curves of the electronic stopping power (blue line) and the nuclear stopping power (red line) distribution, as well as the refractive index profile of the waveguide (green line), as functions of the depth. Parts (b) and (e) show microscopic images of the cross sections of planar and WG2 ridge waveguides, respectively. Experimental [(c), (f)] and simulation [(d), (g)] results of the modal profiles of planar and WG2 ridge waveguides along the TE direction at 1064 nm.

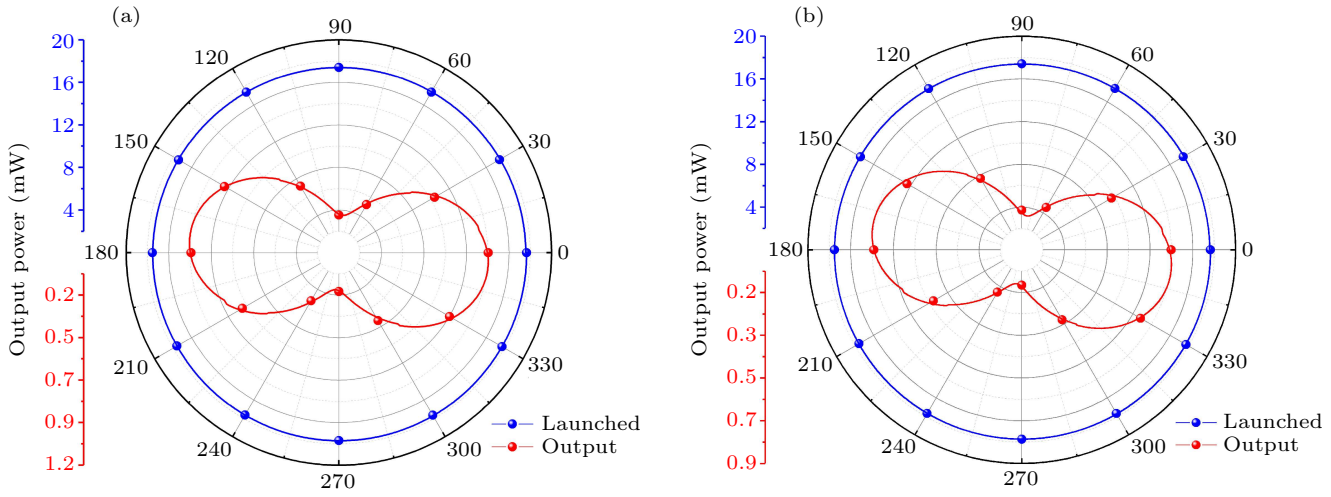


Fig. 4. Output power of (a) planar and (b) WG3 ridge waveguides as a function of all-angle 1064 nm laser transmission with a constant launched power of 17.4 mW under continuous wave configuration.

To investigate the polarization-dependent properties of the waveguides, the all-angle optical transmission of the fabricated waveguide at 1064 nm was measured. As one can see from Fig. 4, for both planar and WG3 ridge waveguides (all the ridge waveguides show similar results), the output power reaches its maxima (0.86 mW and 0.62 mW) along TE polarization (0° and 180°) while decreasing to its minima (0.22 mW and 0.16 mW) along TM polarization (90° and 270°). However, the SHG process occurs under a $TM^{\omega} \rightarrow TE^{2\omega}$ process in Nd:GdCOB waveguides, so the polarization-dependent effect

has a negative impact on the frequency-doubled output power and conversion efficiency of SHG.

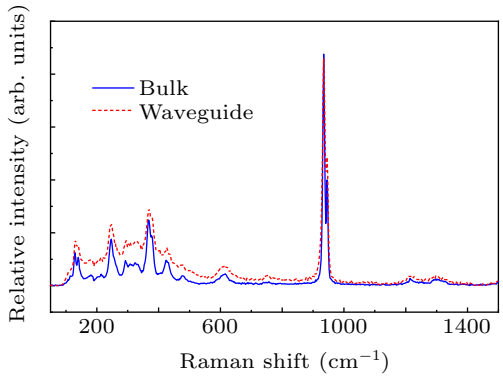


Fig. 5. Micro-Raman spectra obtained from the WG3 ridge waveguide (red dotted line) and the bulk (blue line) of the Nd:GdCOB crystal.

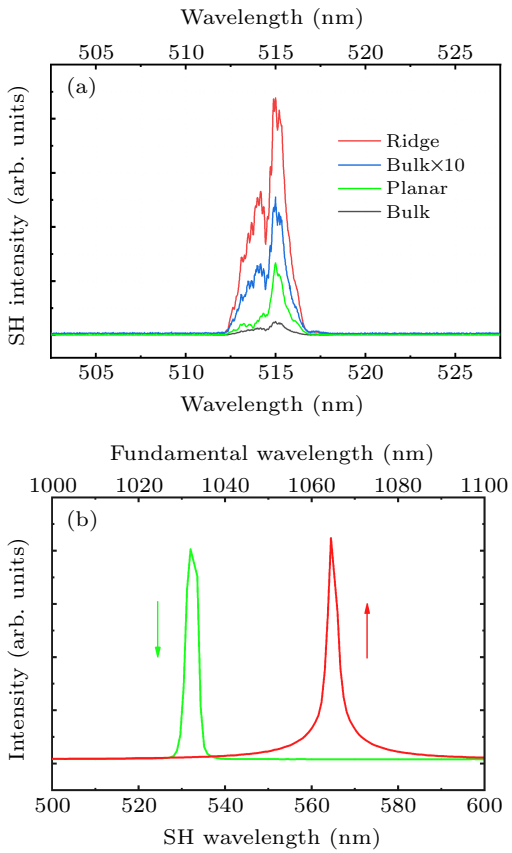


Fig. 6. (a) The emitted intensity of μ-SH spectra when the laser beam (at 1030 nm) is focused at the WG3 ridge waveguide (red line), the planar waveguide (green line) and the bulk (gray line). (b) The laser spectra of the fundamental beam at 1064 nm (red line) and second harmonic generation at 532 nm (green line) in the WG3 ridge waveguide.

Micro-Raman spectra of Nd:GdCOB at the substrate and C^{5+} ion implantation regions are presented in Fig. 5. The Raman peak number and position show no differences between the bulk and waveguide areas. However, the Raman intensity in the waveguide increases with respect to the bulk, which may be a result of the lattice expansion attributed to electronic collisions during ion irradiation.[40–42] It is also possible that C^{5+} ion implantation has caused more point defects in the crystal, leading to a slight broadening of the Raman peak half-width.

The μ-SH responses of the ridge and planar waveguides, as well as the bulk area, were investigated, as shown in Fig. 6(a). From the SH intensity profiles, the intensity distributions for the bulk, planar and ridge waveguides have similar shapes, with their peaks at the same position. However, the SH signal in the WG3 ridge waveguide (all the ridge waveguides show similar results) is enhanced significantly, at around ten times greater than that in the bulk. It is evident that the nonlinear properties of the Nd:GdCOB crystal are well retained and further greatly enhanced in the waveguide. As shown in Fig. 6(b), the spectra measured by the pulsed laser pump of the fundamental (at 1064 nm) and SH (at 532 nm) waves from the WG3 ridge waveguide clearly depict the nonlinear process of SHG in Nd:GdCOB waveguides. The 1064 nm fundamental and SH waves are determined to be TM- and TE-polarized, respectively. This verifies that the SHG process occurs under the $TM^{\omega} \rightarrow TE^{2\omega}$ process, which is in good accordance with the phase matching configuration of the bulk.

Figure 7 illustrates the second harmonic powers (average power) and the conversion efficiencies as functions of the 1064 nm fundamental pump power for planar and WG4 ridge waveguides (WG4 has the best frequency doubling performance of any of the ridge waveguides) under the pulsed configuration. The measured data points are marked with solid circles (blue for the SH powers and red for the conversion efficiencies). For the planar waveguide, the maximum average power output of the SH light is ~ 1.04 mW with a pump power of ~ 112 mW, resulting in a conversion efficiency of $\eta \approx 8.32\ \%{\cdot}W^{-1}$. The maximum average output power of the SH light for the WG4 ridge waveguide is ~ 2.80 mW, which is around two times larger than that of the planar waveguide. The conversion efficiency reaches a maximum value of $\sim 22.36\ \%{\cdot}W^{-1}$, leading to a significantly enhanced performance. An annealing treatment at 260 °C for about 30 min was carried out in order to observe the changes in related nonlinear properties. However, this thermal operation has a negligible influence on the SHG performance of the waveguides. The data on maximum SHG output power (P_{max}), the conversion efficiency (η_{max}) and the propagation losses (α) for all ridge waveguides are summarized in Table 1, and the related properties of the planar waveguide are also included for reference. With an increase in the width of the ridge waveguide, the corresponding maximum SHG power and conversion efficiency will be enhanced. The similar dependence of the SHG properties on the ridge width can also be found in previously reported $KTiOPO_4$ ridge waveguides.[26] Furthermore, ridge waveguides show better performance than planar waveguides in frequency doubling, mainly due to the more compact structure of ridge waveguides, which leads to a stronger light intensity confined in a limited volume. The propagation losses of the ridge waveguides decrease with increase in

ridge width. All ridge waveguides have higher propagation losses than planar waveguide, mainly due to the relatively high waveguide side-wall roughness caused by the dicing process. By optimizing the dicing parameters, such as the blade type and its rotation velocity, the roughness of the waveguide side-wall can be lowered, thereby reducing the propagation loss of the fabricated ridge waveguide.[43] In addition, reduction of the waveguide side-wall roughness can be also realized using ion beam milling.[44] The frequency doubling efficiency will be improved if waveguide losses are optimized, and a self-frequency-doubling effect can be expected.

Table 1. The maximum output SH powers (P_{max}), the maximum conversion efficiencies (η_{max}) and propagation losses (α) of the Nd:GdCOB planar and ridge waveguides.

	WG1	WG2	WG3	WG4	Planar
Width (μm)	10	20	25	30	–
P_{max} (mW)	2.41	2.53	2.68	2.80	1.04
η_{max} (%·W^{-1})	19.22	20.23	21.35	22.36	8.32
α (dB·cm^{-1})	8.5	7.5	7.2	6.9	5.7

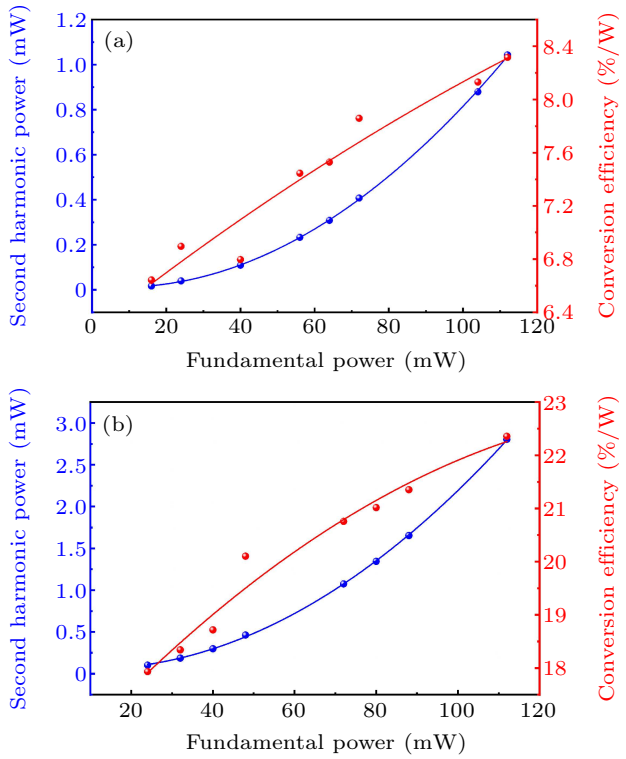


Fig. 7. Second harmonic power and the corresponding conversion efficiency as functions of the fundamental pump power in (a) planar and (b) WG4 ridge waveguides.

4. Conclusion

We have fabricated ridge waveguides in Nd:GdCOB crystals through a combination of carbon ion irradiation and precise diamond blade dicing. Based on an end-face coupling setup, the optical waveguiding properties of both Nd:GdCOB ridge waveguides and planar waveguide were experimentally investigated. The simulated modal profiles agree well with the measurements, suggesting the rationality of the constructed index profile based on stopping powers. From the micro-Raman spectrum, lattice expansion occurs during carbon ion implantation with more point defects. Through μ-SH analysis, the nonlinear properties of the Nd:GdCOB crystal have been found to be fully preserved and greatly enhanced within the waveguides. SHG at 532 nm based on type I phase matching has been observed under a 1064 nm pulsed laser configuration. The maximum SH power of $\sim$ 2.80 mW was obtained in the WG4 ridge waveguide, and the corresponding conversion efficiency was $\sim$ 22.36 %·W^{-1}. For planar waveguide, the maximum SH power was $\sim$ 1.04 mW with a conversion efficiency of 8.32 %·W^{-1}. Our work demonstrates that carbon ion irradiation combined with precise diamond blade dicing can be used to fabricate efficient nonlinear waveguides, providing potential applications in integrated photonics.

Acknowledgments

The authors thank Dr Y. Cheng for waveguide fabrication and Professor H. Yu for μ-SH analysis.

Project supported by the Taishan Scholars Youth Expert Program of Shandong Province and the Qilu Young Scholar Program of Shandong University, China.

References

[1] Jia Y C, Chen F, de Aldana J R V, Akhmadaliev S and Zhou S Q 2012 *Opt. Mater.* **34** 1913
[2] Murphy E J 1999 *Integrated Optical Circuits and Components: Design and Applications* (New York: Marcel Dekker)
[3] Kip D 1998 *Appl. Phys. B: Lasers Opt.* **67** 131
[4] Stegeman G I and Seaton C T 1985 *J. Appl. Phys.* **58** R57
[5] Grivas C 2011 *Prog. Quantum Electron.* **35** 159
[6] Liu Y A, Yan X S, Wu J W, Zhu B, Chen Y P and Chen X F 2020 *Sci. China: Phys., Mech. Astron.* **64** 234262
[7] Jia Y C, Wang S X and Chen F 2020 *Opto-Electron. Adv.* **3** 190042
[8] Chen F 2008 *Crit. Rev. Solid State Mater. Sci.* **33** 165
[9] Jia Y C, Wang L and Chen F 2021 *Appl. Phys. Rev.* **8** 011307
[10] Chen F 2012 *Laser Photonics Rev.* **6** 622
[11] Jia Y C and Chen F 2019 *Chin. Opt. Lett.* **17** 012302
[12] Chen F, Amekura H and Jia Y C 2020 *Ion Irradiation of Dielectrics for Photonic Applications* (Singapore: Springer Nature) p. 6
[13] Wesch W and Wendler E 2016 *Ion Beam Modification of Solids* (Cham: Springer Nature) p. 153
[14] Li Z Q and Chen F 2017 *Appl. Phys. Rev.* **4** 011103
[15] Townsend P D, Chandler P J and Zhang L 1994 *Optical Effects of Ion Implantation* (Cambridge: Cambridge University Press)
[16] Chen F, Wang X L and Wang K M 2007 *Opt. Mater.* **29** 1523
[17] Chen F 2009 *J. Appl. Phys.* **106** 081101
[18] Bentini G G, Bianconi M, Chiarini M, Correra L, Sada C, Mazzoldi P, Argiolas N, Bazzan M and Guzzi R 2002 *J. Appl. Phys.* **92** 6477
[19] Jia Y C, Rüter C E, Akhmadaliev S, Zhou S, Chen F and Kip D 2013 *Opt. Mater. Express* **3** 433
[20] Jia Y C, Tan Y, Cheng C, Aldana J R V d and Chen F 2014 *Opt. Express* **22** 12900
[21] Jia Y C, Dong N N, Chen F, de Aldana J R V, Akhmadaliev S and Zhou S Q 2012 *Opt. Mater. Express* **2** 657
[22] Siebenmorgen J, Petermann K, Huber G, Rademaker K, Nolte S and Tünnermann A 2009 *Appl. Phys. B: Lasers Opt.* **97** 251
[23] Okhrimchuk A G and Shestakov A V 2005 *Opt. Lett.* **30** 2248
[24] Chen F and de Aldana J R V 2014 *Laser Photonics Rev.* **8** 251
[25] Cheng Y Z, Lv J M, Akhmadaliev S, Zhou S Q, Kong Y F and Chen F 2015 *Opt. Mater.* **48** 209

[26] Chen C, Ruter C E, Volk M F, Chen C, Shang Z, Lu Q M, Akhmadaliev S, Zhou S Q, Chen F and Kip D 2016 *Opt. Express* **24** 16434

[27] Lu J H, Li G M, Liu J H, Zhang S J, Chen H C, Jiang M H and Shao Z S 1999 *Opt. Commun.* **168** 405

[28] Wang C Q, Chow Y T, Gambling W A, Zhang S J, Shao Z S and Chen H C 2000 *Opt. Commun.* **174** 471

[29] Mougel F, Aka G, Kahn-Harari A, Hubert H, Benitez J M and Vivien D 1997 *Opt. Mater.* **8** 161

[30] Aka G, Mougel F, Auge F, Kahn-Harari A, Vivien D, Benitez J M, Salin F, Pelenc D, Balembois F, Georges P, Brun A, Nain N L and Jacquet M 2000 *J. Alloys Compd.* **303–304** 401

[31] Du J H, Wang J Y, Yu H H and Zhang H J 2019 *Opt. Lett.* **45** 327

[32] Ren Y Y, Jia Y C, Chen F, Lu Q M, Akhmadaliev S and Zhou S Q 2011 *Opt. Express* **19** 12490

[33] Jia Y C, de Aldana J R V, Lu Q M, Jaque D and Chen F 2013 *J. Lightwave Technol.* **31** 3873

[34] Disco Co.

[35] Zhang J, Chen J Y, Lu Y, Wang Y S, Zhang L L, Yue Q Y, Zheng R L and Liu C X 2021 *Vacuum* **193** 110493

[36] Zhou Y F, Wang L, Liu P, Liu T, Zhang L, Huang D T and Wang X L 2014 *Nucl. Instrum. Methods Phys. Res., Sect. B* **326** 110

[37] Zhao J H, Jiao X S, Ren Y Y, Gu J J, Wang S M, Bu M Y and Wang L 2021 *Chin. Opt. Lett.* **19** 060009

[38] Ziegler J F 2012 Computer code *SRIM*

[39] RSoft Design Group 2013 Computer software *BeamPROP*

[40] He S, Zhang Z, Liu H, Akhmadaliev S, Zhou S, Wang X and Wu P 2019 *Applied Physics Express* **12** 076502

[41] Pandey P, Bitla Y, Zschornak M, Wang M, Xu C, Grenzer J, Meyer D C, Chin Y Y, Lin H J, Chen C T, Gemming S, Helm M, Chu Y H and Zhou S 2018 *APL Materials* **6** 066109

[42] Chen C, Wang C, Cai X, *et al.* 2019 *Nanoscale* **11** 8110

[43] Volk M F, Rüter C E, Santandrea M, Eigner C, Padberg L, Herrmann H, Silberhorn C and Kip D 2018 *Opt. Mater. Express* **8** 82

[44] Degl'Innocenti R, Reidt S, Guarino A, Rezzonico D, Poberaj G and Günter P 2006 *J. Appl. Phys.* **100** 113121